Simulation of stratification phenomena with a spectral Fourier–Chebyshev method on the background of a lead-cooled fast reactor☆

Daxiao Liu [a,b,c], Philipp G. Marthaler [c], Andreas G. Class [c,*], Long Gu [a,b,d,**]

[a] Institute of Modern Physics, Chinese Academy of Sciences, Lanzhou, China
[b] School of Nuclear Science and Technology, University of Chinese Academy of Sciences, Beijing, China
[c] Institute for Thermal Energy Technology and Safety, Karlsruhe Institute of Technology, Karlsruhe, Germany
[d] School of Nuclear Science and Technology, Lanzhou University, Lanzhou, China

ARTICLE INFO

Keywords:
Stratification
Spectral Fourier and Chebyshev method
Lead-cooled fast reactor (LFR)
POD-ROM

ABSTRACT

Thermal stratification in the upper plenum of the lead-cooled fast-reactor under SCRAM conditions can cause material fatigue and failure of elements critical for reactor safety. Adapting the reactor design to resist the thermohydraulic loads is an ongoing challenge addressed by a large range of experimental and numerical studies. A promising numerical approach for the efficient computation of the highly dynamic fluid behaviors in the complex geometry of the upper plenum is POD-ROM (Reduced-Order Modeling via Proper Orthogonal Decomposition). Therefore, calibration with a high-accurate solution showing the relevant physical effects is necessary. We present a spectral code capable of performing the calibration due to its high accuracy. The code which is based on the combination of Fourier and Chebyshev modes is applied to a 2D example system to show the ability for thermal stratification research. Verification is performed by computing Rayleigh–Bénard convection.

1. Introduction

The lead-cooled fast reactor (LFR) is applied by the China Initiative Accelerator Driven Systems (CiADS) (Peng et al., 2017) due to its good nuclear waste transmutation and nuclear fuel breading ability. A 3D model of the reactor type is depicted in Fig. 1. A matter of ongoing investigations and a crucial safety issue is the appearance of thermal stratification in the primary components of the reactor, such as core, upper and lower plenum. The thermal-hydraulic design of the reactor is supposed to minimize stratification and its effects (Tenchine et al., 2013).

In our work we concentrate on thermal stratification in the upper plenum under scram conditions. The decelerating coolant flow from the core upwards into the upper plenum is superimposed with an axial temperature difference. The resulting pulsating waves at the stratification interface cause oscillations also in the reactor elements. In addition to the failure of these elements (Das et al., 2012), further effects can cause serious and unpredictable situations. The characteristics of the nuclear system can change (Opanasenko et al., 2012) and the heat removal system which is based on natural convection can fail (Tenchine, 2010).

The problem of stratification in the upper plenum has been addressed by a range of experimental investigations, such as E-SPACE, TALL, HELLOS (Visser et al., 2020; Sehgal and Ma, 2006; Lee and Suh, 2006). Authors agree on the necessity of a numerical solver that can handle the multi-physical, multi-scale (because of the emergence of anisotropic turbulence) and the complex geometry of the upper plenum. CFD methods and Coupling System-level via CFD Methods are applied to predict thermal stratification phenomenon in Liquid metal reactors (Ohno et al., 2011; Ohira et al., 2013a; Sakamoto et al., 2010; Bandini et al., 2015). Due to the different heat transport behavior of a liquid metal compared to a fluid like air or water, liquid metal turbulence challenges the heat transport models (Roelofs et al., 2013). It is essential for the buoyancy term in thermal stratification simulation. Researching internal waves due to oscillations requires high resolution results of turbulence behaviors (Opanasenko, 1988), which is vital for thermal fatigue research. Advanced numerical tools are required for further research.

The development of computing technology provides a good opportunity for the next generation of CFD using spectral methods. The

☆ This work was supported by the DAAD scholarship, the Research on key technology and safety verification of primary circuit, Grant No. 2020YFB1902104, the Experimental study on thermal hydraulics of fuel rod bundle, Grant No. Y828020XZ0 and the National natural science foundation of China, Grant No. 12122512.
* Corresponding author at: Institute for Thermal Energy Technology and Safety, Karlsruhe Institute of Technology, Karlsruhe, Germany.
** Corresponding author at: Institute of Modern Physics, Chinese Academy of Sciences, Lanzhou, China.

E-mail addresses: andreas.class@kit.edu (A.G. Class), gulong@impcas.ac.cn (L. Gu).

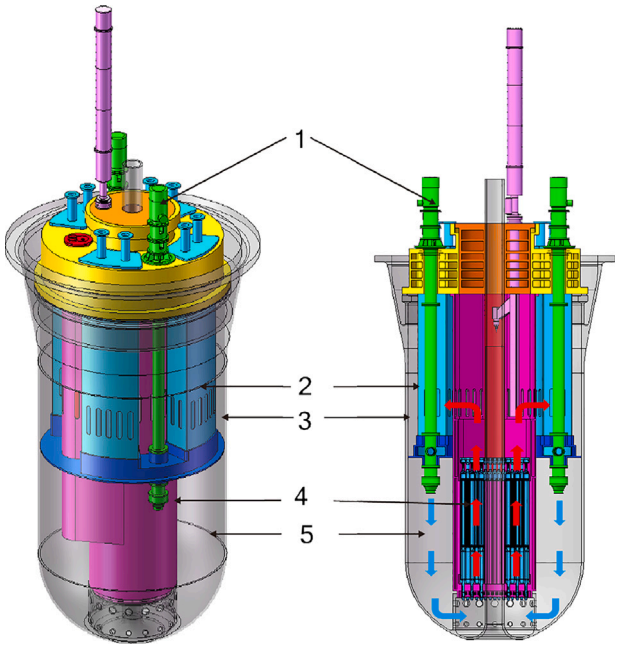

Fig. 1. Schematic figure of LFR vessel (1)pump, (2) IHX outlet, (3) upper plenum, (4) core, (5) lower plenum.

NEK5000, a spectral element method code, can handle complex geometry by sacrificing the accuracy, compared with the pure spectral method. The discussion of massive multiscale separation was conducted with the NEK5000 in nuclear reactors by Argonne National Laboratory (ANL) (Merzari et al., 2017). The Another promising approach to efficiently model thermal stratification is Reduced Order Modeling (ROM), which uses a relatively small number of solutions generated by a high fidelity CFD calculation to construct a computationally tractable model. A reduced order three-dimensional module is under development for thermal mixing and stratification modeling, which is part of the system analysis module (SAM) developed at ANL (Hu, 2017). The Reduced-Order Modeling via Proper Orthogonal Decomposition (POD-ROM) verification of a simulation in a heated pool was performed to study natural convection in nuclear reactors (Yanez and Class, 2019). Our work will finally concentrate on the development of a spectral method code that can provide high fidelity results for the ROM methods in order to provide a reliable and efficient numerical simulation module for nuclear energy development.

A number of authors studied of similar problems using a variety of spectral methods to understand the e.g. oscillations or horizontal convection with long-living vortices (Wu et al., 2018; Cai, 2016; Alam et al., 2009). Our approach combines the methods of Fourier collocation and Chebyshev-tau and computes the solution of the boundary-value problem in spectral space. The necessary transformations are preformed with FFT-based modules which make the code not only accurate but also efficient.

2. A reduced model of the upper plenum for high-accuracy simulations of stratification

Stratification in the upper plenum during SCRAM has been observed in a number of experiments (Anon, 1993). Due to the high dynamics of stratification phenomena the appearance of such behavior is critical for safety systems and gives rise to many uncertainties. In order to understand the effects of stratification experiments and numerical simulations have been performed (Ohira et al., 2013b; Sehgal and Ma, 2006; Lee and Suh, 2006; Visser et al., 2020).

The fluid mechanical conditions under which stratification appears can be mainly characterized by a decelerating convective flow of the coolant from the core upwards into the upper plenum. The interaction of heat difference and convection results in stratified interface in the volume. The location of their interface as well as the emerging forces are time-variant and complex. In Fig. 2(a) a schematic snapshot of such a condition is displayed.

High-accuracy simulations of such behavior in the complex geometry of the reactor are (if feasible) very costly. Thus, a number of experimental and numerical investigations mentioned above (Ohira et al., 2013b; Sehgal and Ma, 2006; Lee and Suh, 2006; Visser et al., 2020) have made simplifications mainly utilizing the symmetry of the upper plenum. In such setups the inner components are reorganized to fulfill the symmetry. With experiments/simulations using the 2D model as displayed in Fig. 2(b) stratification has been observed (Ohira et al., 2013b; Moriya et al., 1987; Langhans, 2017).

For the application of a POD-ROM code, which has been applied for different applications for the complex geometry problem , a highly accurate solution exhibiting the relevant physical phenomena is required (Hesthaven et al., 2016). Spectral method are a suitable method to compute such a solution as their error decreases exponentially with the number of collocation points used. The high-accurate results will be used as snapshots of the POD-ROM code. Thereby the relevant modes for the problem are identified so that settings with much more complex behavior and geometry can be investigated in detail.

Performing two further reduction steps on the model from Fig. 2(b) we receive a model that is showing the essential phenomenon of layering and the dynamics of stratification and is at the same time simple enough to be computed efficiently with spectral methods. In the first step we reduce the geometry to a simple box with in- and outlet at the same positions as before. At the top and bottom wall the temperature boundary conditions T_1^* and T_0^* are applied[1] (Compare Fig. 2(c)). In a second step we use a periodic grid in the x-direction arranging in- and outlet at the bottom wall (see Fig. 3). The constant velocity profile at inlet and outlet is characterized by the velocity v_{ref}^*. The length scale of the problem is given by the distance between upper and lower wall. Density ρ_0^*, kinematic viscosity μ^*, heat capacity c_p^* and heat conduction coefficient κ are assumed to be constant in the considered domain and time. The buoyancy force is modeled with the Boussinesq approximation using the heat expansion β. Thus, the dynamic viscosity is $\nu^* = \mu^*/\rho_0^*$ and the heat diffusion is $\alpha^* = \kappa^*/\rho_0^* c_p^*$.

The fluid dynamical problem is governed by the conservation equations for momentum and mass. The system is assumed to be incompressible and 2D. The energy equation complements the set of equations

$$\begin{aligned} \frac{\partial \theta}{\partial t} + \left(\vec{v}\cdot\nabla\right)\theta &= \frac{1}{\mathrm{Pe}}\nabla^2\theta, \\ \frac{\partial \vec{v}}{\partial t} + \left(\vec{v}\cdot\nabla\right)\vec{v} &= -\nabla p + \frac{1}{\mathrm{Re}}\nabla^2\vec{v} + \mathrm{Ri}\,\theta\,\vec{e}_y, \\ \nabla\cdot\vec{v} &= 0. \end{aligned} \tag{1}$$

The velocity is scaled with the reference velocity of the inlet flow $\vec{v}(x,y,t) = (u(x,y,t), v(x,y,t))^{\mathsf{T}} = \vec{v}^*/v_{\mathrm{ref}}^*$ and the dimensionless temperature is defined by $\theta(x,y,t) = \left(\theta^*(x,y,t) - T_0^*\right)/\left(T_1^* - T_0^*\right)$. With the length scale l_{ref}^*, which is the distance between upper and lower wall, we define the time scale $t_{\mathrm{ref}}^* = l_{\mathrm{ref}}^*/v_{\mathrm{ref}}^*$. The Richardson number $\mathrm{Ri} = \left(\beta^* g^* l_{\mathrm{ref}}^* \left(T_1^* - T_0^*\right)\right)/{v_{\mathrm{ref}}^*}^2$ is defined as the ratio between buoyancy and convective forces. The scaling is complemented by the Reynolds number $\mathrm{Re} = \left(v_{\mathrm{ref}}^* l_{\mathrm{ref}}^*\right)/\nu^*$ and the Péclet number $\mathrm{Pe} = \left(v_{\mathrm{ref}}^* l_{\mathrm{ref}}^*\right)/\alpha^*$, which can be combined to the Prandtl number $\mathrm{Pr} = \mathrm{Pe}/\mathrm{Re} = \nu^*/\alpha^*$.

By introducing the streamfunction $\psi(x,y,t)$ with $\partial\psi/\partial y = u$ and $\partial\psi/\partial x = -v$ we can reduce the number of equations from four to two.

[1] Parameters with dimensions are denoted by $(..)^*$.

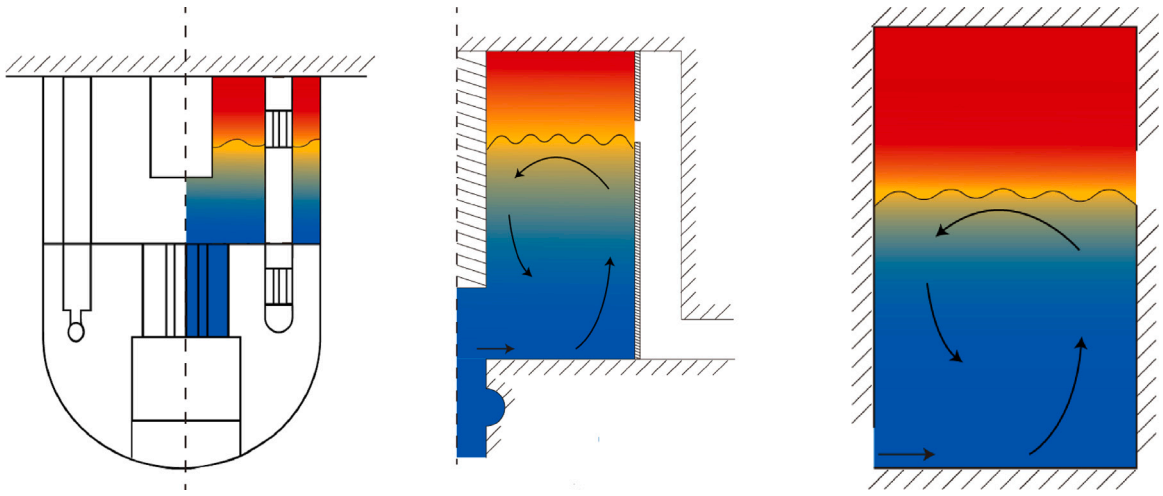

Fig. 2. (a) reactor model with relevant section in the upper plenum colored. (b) experimental setup with symmetry assumptions. (c) cavity with inlet and outlet as reduction to the experimental setup. Coolant's estimated temperature is depicted by colors.

The streamfunction is defined to fulfill the continuity equation. By applying the rotation operator two times to the momentum conservation the pressure term vanishes and we find

$$\begin{aligned} \frac{\partial \theta}{\partial t} + \left(\vec{v}\cdot\nabla\right)\theta &= \frac{1}{\mathrm{Pe}}\,\nabla^2\theta, \\ \frac{\partial}{\partial t}\nabla^2\psi + (\vec{v}\cdot\nabla)\nabla^2\psi &= \frac{1}{\mathrm{Re}}\,\nabla^4\psi - \mathrm{Ri}\,\frac{\partial\theta}{\partial x}. \end{aligned} \tag{2}$$

The biharmonic operator is defined as $\nabla^4 = \nabla^2\nabla^2 = \partial_{xxxx} + \partial_{yyyy} + 2\partial_{xxyy}$.

The set of nonlinear partial differential equations we receive is of fourth order. It is solved together with the boundary conditions in dimensionless form

$$\begin{aligned} \theta\,(x=0,y,t) &= 0, \\ \theta\,(x=1,y,t) &= 1, \\ \psi\,(x=0,y,t) &= \psi_0\,(y,t), \\ \psi\,(x=1,y,t) &= 0. \end{aligned} \tag{3}$$

To fulfill the inlet and outlet boundary conditions the streamfunction at the lower wall is given as

$$\psi_0\,(x,t) = \delta\,(t)\,\omega\,(x),$$

where

$$\delta\,(t) = \tanh\,(0.03t),$$

$$\omega\,(x) = \begin{cases} 0 & -\frac{l_1}{2} \le x < -l_3 - \frac{l_2}{2} \\ x + l_3 + \frac{l_2}{2} & -l_3 - \frac{l_2}{2} \le x < -\frac{l_2}{2} \\ l_3 & -\frac{l_2}{2} \le x < \frac{l_2}{2} \\ -x + l_3 + \frac{l_2}{2} & \frac{l_2}{2} \le x < \frac{l_2}{2} + l_3 \\ 0 & \frac{l_2}{2} + l_3 \le x < \frac{l_1}{2}. \end{cases} \tag{4}$$

As initial conditions, the streamfunction is set to null in the whole domain (which is equal to vanishing pressure and velocity). For the temperature boundary condition of top wall is given.

$$\begin{aligned} \psi\,(x,y,t=0) &= 0, \\ \theta\,(x,y,t=0) &= \theta\,(x=1,y,t). \end{aligned} \tag{5}$$

3. Numerical solution with a 2D Fourier-Chebyshev spectral method

The accuracy of spectral methods is illustrated exemplary of the Fourier collocation method. A generic boundary value problem $A\,(f\,(x,t)) = \vec{b}$ is solved during numerical computations to find the solution $f\,(x,t)$. This can be approximated by a series expansion

$$f_N\,(x,t) = \sum_{k=1}^{N} \tilde{f}_k(t)\varphi_k(x) \tag{6}$$

truncated after the Nth element. We demand the resulting error $A(f_N) - b$, multiplied with a weight function $w(x)$, to vanish

$$\int_\Omega w(x)\left(A(f_N) - b\right)\mathrm{d}x = 0. \tag{7}$$

Using the collocation weight $w(x) = \delta\left(x - x_i\right)$ with the Dirichlet distribution, we demand the residual at each grid point x_k in the domain Ω to be null. This explains the high accuracy of the method. The periodic trial functions $\varphi_k(x) = \exp\left(\mathrm{i}kx\right)$ lead to a Fourier spectral method. In that case, the relation (6) gives the transformation between Fourier coefficients $\tilde{f}_k$ for the single and the physical parameters f_i at the grid points x_i.

For the Chebyshev method a similar transformation relation can be applied. We define the spectral coefficients (denoted with tildes) as the spectral transform of the physical values

$$\tilde{f}_{kl} = \mathcal{T}\left\{f_{ij}\right\}, \tag{8}$$

with i and j denoting the grid point at which the value f_{ij} is located and k and l denoting the modes. For the Fourier modes in the periodic x-direction we use an equidistant grid $x_i = i\Delta x$, $i = 0, \ldots, N_x$. For the Chebyshev modes we introduce Gauss–Lobatto points in the y-direction which are defined as $x_j = {}^{2\pi j}/_{N_y}, i = 0, \ldots, N_y$. The Gauss–Lobatto points lie closer together close to the boundaries and are more distant in the middle of the domain. The number of modes k and l are equal to the numbers of grid points N_x and N_y respectively. The grid for our domain is displayed in Fig. 4. We can also find the back transformation

$$f_{ij} = \mathcal{T}^{-1}\left\{\tilde{f}_{kl}\right\}. \tag{9}$$

During the computation the set of equations (2) is transformed to the spectral space where it is solved for each time step. The results of interest can be transformed back to physical space. The back transform is also needed for the nonlinear terms as they cannot be computed in spectral space. The relevant values have to be transformed to physical space at each time step where the nonlinear terms can be computed and then transformed back to spectral space. As an alternative to the very costly direct transforms with complexity $O(N^2)$ both, the Fourier and the Chebyshev transform, can be performed with the FFT (Fast Fourier Transform) with complexity $O(5N\log_2(N))$.

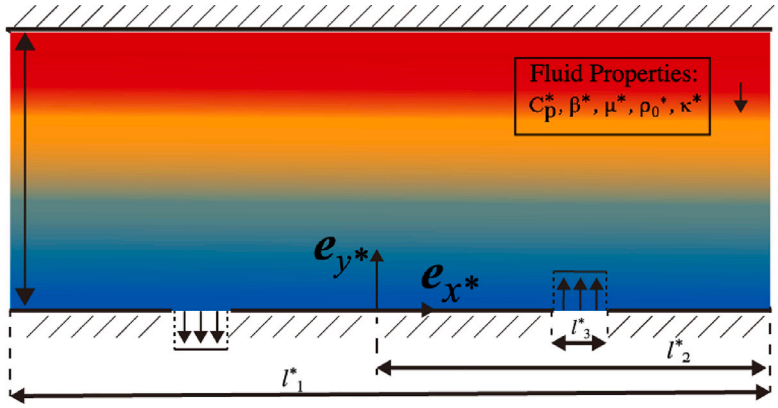

Fig. 3. Model and parameters of the investigated problem. The domain is assumed periodic in x-direction. The upper wall is heated, inlet and outlet are arranged inside the bottom wall.

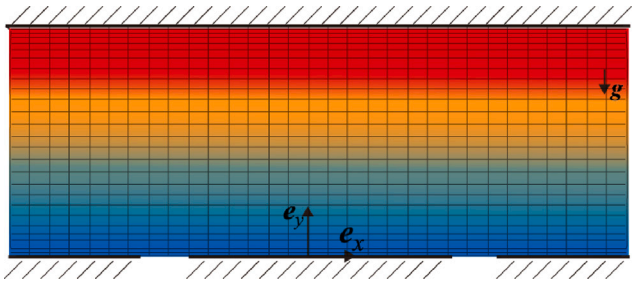

Fig. 4. Grid lines for the combined spectral method. The lines in x-direction for the Fourier method are equidistant, the Gauss–Lobatto distribution in y-direction is not. The lines are closer together at the walls and far from each other in the middle of the domain.

The set of equations (2) is transformed into the spectral form

$$\begin{aligned} \frac{\partial}{\partial t}\tilde{\theta}_{kl} &= \frac{1}{\mathrm{Pe}}\tilde{\nabla}^2\tilde{\theta}_{kl} + \tilde{C}_\theta, \\ \frac{\partial}{\partial t}\tilde{\nabla}^2\tilde{\psi}_{kl} &= \frac{1}{\mathrm{Re}}\tilde{\nabla}^4\tilde{\psi}_{kl} + \tilde{C}_\psi + \tilde{B}_\psi. \end{aligned} \tag{10}$$

The nonlinear convection terms C and the buoyancy term B_ψ which have to be treated individually are defined as

$$\begin{aligned} \tilde{C}_\theta &= -\left(\tilde{\vec{v}}_{kl}\cdot\tilde{\nabla}\right)\tilde{\theta}_{kl}, \\ \tilde{C}_\psi &= -(\tilde{\vec{v}}_{kl}\cdot\tilde{\nabla})\tilde{\nabla}^2\tilde{\psi}_{kl}, \\ \tilde{B}_\psi &= -\,\mathrm{Ri}\,\tilde{\partial}_x\tilde{\theta}_{kl}, \end{aligned} \tag{11}$$

For the energy equation we use the Euler implicit time scheme. For the streamfunction equation we use a second order composite time scheme which can be displayed also as Euler implicit in the formulation we use. For the nonlinear terms, an explicit time scheme has to be applied. We found an Adams–Bashforth method to be the best deal between cost and numerical stability. The equations with the time discretization $t^n = n\Delta t$ applied are

$$\begin{aligned} \left(\mathcal{I} - \frac{\Delta t}{\mathrm{Pe}}\tilde{\nabla}^2\right)\tilde{\theta}^n_{kl} &= \tilde{\nabla}^2\tilde{\theta}^{n-1}_{kl} + \Delta t\left(2\tilde{C}^{n-1}_\theta - \tilde{C}^{n-2}_\theta\right), \\ \left(\tilde{\nabla}^2 - \frac{\Delta t}{\mathrm{Re}}\tilde{\nabla}^4\right)\tilde{\psi}^n_{kl} &= \tilde{\nabla}^2\tilde{\psi}^{n-1}_{kl} \\ &\quad + \Delta t\left(2\tilde{C}^{n-1}_\psi - \tilde{C}^{n-2}_\psi\right) + \Delta t\tilde{B}^n_\psi. \end{aligned} \tag{12}$$

At each time step the energy equation is solved first and delivers the value $\tilde{\theta}^n_{kl}$ which can be utilized to compute the buoyancy term $\tilde{B}^n_\psi$ at the regarding time step n.

The boundary conditions are transformed into spectral space as well.

During validation we found the relative errors of the code at single precision to be of maximum size 10^{-12}. Verification is performed using the Rayleigh–Bénard convection as an example in Section 4. Afterwards the results for our model are discussed in Section 5.

4. Code verification on Rayleigh–Bénard convection

The case of Rayleigh–Bénard convection which has been intensively investigated by a large number of authors (Bodenschatz et al., 2000; Bruyn et al., 1996; Gershuni and Zhukhovitskii, 1969; Busse, 1989) in the past is utilized as a verification example to demonstrate the applicability of our code. Rayleigh–Bénard convection can be observed between two solid walls from which the lower one is heated. The heat transport in this system can be performed in form of heat conduction or convection. (In the convective state heat conduction through the fluid is still existent but significantly less important than the convective transport.) How the system behaves is mainly dependent on the Rayleigh number which is the ratio of buoyancy and viscous forces and is defined below for our system. When the Rayleigh number or the heat difference (they are linearly related) becomes larger than a critical value the motionless conductive state is turning into heat convection showing the characteristic cellular behavior.

We can easily modify our model to investigate Rayleigh–Bénard convection. We neglect the in- & outlet and turn around the heat difference. The system is now heated from bottom instead from top. The periodic boundary conditions in x-direction fit perfectly to observe the periodic behavior of the system. With the removal of the inlet we define a new reference velocity $v^*_{\mathrm{ref}} = \nu/l^*_{\mathrm{ref}}$. Thus, from the Richardson number arises the Rayleigh number $\mathrm{Ra} = \left(\rho^* g^* {l^*_{\mathrm{ref}}}^3\left(T^*_1 - T^*_0\right)\right)/\nu^{*2}$, the Reynolds number becomes unity and vanishes from the equations and the Péclet and Prandtl numbers become equal $\mathrm{Pe} = \mathrm{Pr} = \nu^*/\alpha^*$. The basic set of Eqs. (2) and the boundary conditions (3) are transformed into

$$\begin{aligned} \frac{\partial\theta}{\partial t} + \left(\vec{v}\cdot\nabla\right)\theta &= \frac{1}{\mathrm{Pr}}\nabla^2\theta, \\ \frac{\partial}{\partial t}\nabla^2\psi + (\vec{v}\cdot\nabla)\nabla^2\psi &= \nabla^4\psi - \mathrm{Ra}\,\frac{\partial\theta}{\partial x}, \\ \theta(x=0,y) = 0 \quad &\text{and} \quad \theta(x=1,y) = 1, \\ \psi(x=0,y) = 0 \quad &\text{and} \quad \psi(x=1,y) = 0. \end{aligned} \tag{13}$$

The no-flow initial condition is stable. Small perturbations of the initial state lead to the stationary behavior of Rayleigh–Bénard. The small perturbations are modeled with white noise. We found that amplitudes of the noise of order 10^{-5} are work very well in this context.

The critical Rayleigh number can be identified by a linear stability analysis to be $\mathrm{Ra}_c = 1708$ for no-slip boundary conditions at the walls (Ingersoll, 1966; Baranowski and Kawczyński, 1972; Aurnou and Olson, 2001). The heat conduction state exists independently of the Prandtl number of the fluid below this critical value. For Rayleigh numbers $\mathrm{Ra} > \mathrm{Ra}_c$ the flow, e.g. characterized by the maximum velocity shows different behaviors for different fluids. In the bifurcation diagram (Fig. 5) this behavior was successfully computed by our code.

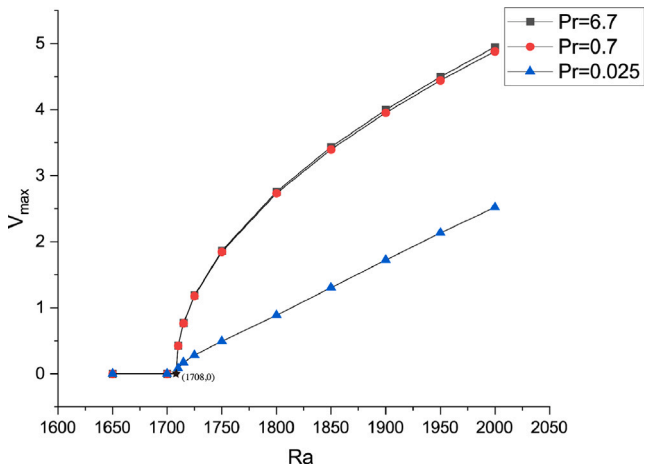

Fig. 5. The maximum velocity as a function of the Rayleigh number.

5. The analysis of the key dimensionless numbers for the stratification

The investigated system can be characterized by the three dimensionless numbers Ri, Re and Pr. While the Prandtl number is defined by the choice of the medium, the other two depend on the outer conditions like length scale, inlet velocity and temperature difference. Reynolds numbers are considered to be in the range of $\mathrm{Re} \in [1, 100]$. The lower limit is typical for natural convection as discussed in Section 4. The higher limit refers to an inlet velocity which is higher by two orders. Richardson number is in the range of $\mathrm{Ri} \in [50, 2000]$ according to the typical experiment value (Ieda et al., 1990).

We find out the blocking phenomenon, which occurs when the potential energy barrier caused by the density variation is larger than the dynamic head of fluid. This mechanization results in two layers for the distribution of velocity. In the lower part, the flow is dominated by convection. In the upper layer, the fluid is nearly motionless. We define the parameter of interest as the vertical position of the interface of the two layers y_{strat}, which is related to the three input parameters of the simulation. To compute this value, we define an auxiliary variable

$$\psi_{j,\mathrm{strat}} = \sum_{i}^{N_x} \left| \psi_{ij} - \bar{\psi}_j \right|, \tag{14}$$

which describes, how wavy the streamlines at one horizontal row of grid points are. The mean value $\bar{\psi}_j$ of the streamfunction in one horizontal row is computed in a preceding step. The operator $|..|$ denotes the absolute value. The stratification position can then be found as

$$y_{\mathrm{strat}} = y_j \quad \left\{ j : \psi_{j,\mathrm{strat}} < \varepsilon \wedge \max \right\}. \tag{15}$$

When one considers $\psi_{j,\mathrm{strat}}$ as the waviness of the streamlines at the position j, the stratification interface is defined as the position at which the waviness is below a threshold ε. Thus, a range of $\psi_{j,\mathrm{strat}}$ fulfilling this condition can be found, namely all values lying inside the upper layer. Therefore, we choose the location y_j which has the lowest vertical position as stratification position y_{strat}.[2]

Fig. 6 shows the system behavior for a typical parameter combination. According to the velocity distribution from point A to point E, the buoyancy caused by the temperature difference has a significant effect on the flow state. On the initial state A, since the computational domain does not have a temperature difference, the flow field distribution is dominated by convection terms and viscous dissipation terms. With the given θ at the lower boundary, buoyancy gradually becomes the dominant factor, which has a significant inhibitory effect on velocity distribution. The result reveals that thermal stratification may inhibit natural circulation under an emergency shutdown condition, which causes the failure of residual heat removal. In this case, the large temperature gradient on the interface does not occur due to the improper aspect ratio. The thermal conduction is still strong enough to interrupt the occurrence of temperature stratified layers.

The y_{strat} changing with Ri and Re number in $\mathrm{Pr} = 0.025$ is displayed in 7. When Re number < 25, the small Penumber means that the diffusion term dominates temperature development. The diffusion velocity scale(α/L) is much larger than the convection scale, resulting in decoupling of the momentum equation and the energy equation. When Re gradually increases, the number of Ri will be the dominant parameter of y position, which is consistent with the experimental results (Ieda et al., 1990).

6. Outlook

We developed a 2D spectral Fourier–Chebyshev code capable of researching stratification phenomena. Validation showed a relative accuracy of the order 10^{-12}. The code was verified on the Rayleigh–Bénard problem, delivering the typical bifurcation behavior. The critical Ra_c under no-slip boundary condition is captured accurately with our code. The influences of inlet flow, temperature difference, and fluid on the stratification interface have been investigated and appear physical. The code gives the temperature and velocity distribution with time development, which influences buoyancy on the fluid velocity and temperature distribution under thermal stratification conditions.

Further investigations are supposed to deal with an enclosed cavity as depicted in Fig. 2(c) instead of the periodic computational domain. A fitting aspect ratio can show more details of behaviors of temperature stratified layers. Also, time-dependent inlet flow has to be considered, probably resulting in the oscillatory behavior which was discussed in the introduction. Thus, the stratification can be modeled more detailed.

At the same time, the calibration of the POD-ROM code can be performed. The first verification with experimental results is possible. The thickness of the temperature boundary layer is more significant than that of the velocity boundary layer because liquid metal has the smallPr number (~0.025). The high-order spectral method solver with the LES/DNS turbulence model will be further developed to study high-precision numerical solutions of liquid metal flow and heat transfer problems.

CRediT authorship contribution statement

Daxiao Liu: Code development, Solver establishment, Formal analysis, Writing – review & editing. **Philipp G. Marthaler:** Code development, Writing – original draft. **Andreas G. Class:** Conceptualization, Methodology. **Long Gu:** Conceptualization, Funding acquisition.

Declaration of competing interest

The authors declare that they have no known competing financial interests or personal relationships that could have appeared to influence the work reported in this paper.

Data availability

Data will be made available on request.

[2] Due to the definition of the Gauss–Lobatto points (cp. Section 3) the lowest y_j corresponds to the highest index j.

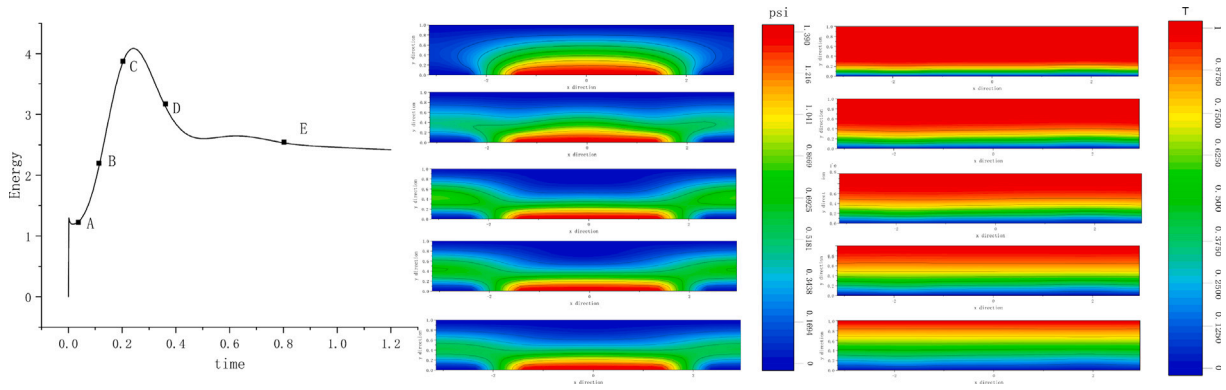

Fig. 6. The system behavior for Re = 1, Pr = 1 and Ri = 2000 Left: Energy changes over time. Middle: The streamfunction distributions on the specific time from A to E. Right: The temperature distributions on the specific time from A to E.

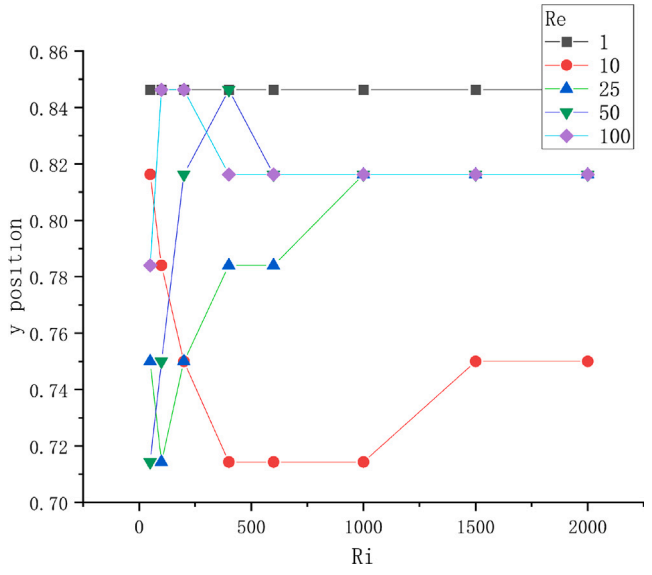

Fig. 7. The y position of lowest velocity as a function of Ri number.

References

Alam, Mohammad-Reza, Liu, Yuming, Yue, Dick K.P., 2009. Waves due to an oscillating and translating disturbance in a two-layer density-stratified fluid. J. Eng. Math. 65 (2), 179–200.

Anon, 1993. Specialists's meeting on evaluation of decay heat removel by natural convection. JAPAN.

Aurnou, J.M., Olson, P.L., 2001. Experiments on Rayleigh–Bénard convection, magneto-convection and rotating magnetoconvection in liquid gallium. J. Fluid Mech. 430, 283.

Bandini, G., et al., 2015. Assessment of systems codes and their coupling with CFD codes in thermal–hydraulic applications to innovative reactors. Nucl. Eng. Des. 281, 22–38.

Baranowski, B., Kawczyński, A.L., 1972. Experimental determination of the critical Rayleigh number in electrolyte solutions with concentration polarization. Electrochim. Acta 17 (4), 695–699.

Bodenschatz, Eberhard, Pesch, Werner, Ahlers, Guenter, 2000. Recent developments in Rayleigh-bénard convection. Annu. Rev. Fluid Mech. 32 (1), 709–778.

Bruyn, D., John, R., Bodenschatz, et al., 1996. Apparatus for the study of Rayleigh-benard convection in gases under pressure. Rev. Sci. Instrum.

Busse, F.H., 1989. Fundamentals of thermal convection. In: Peltier, W.R. (Ed.), Mantle Convection: Plate Tectonics and Global Dynamics. Gordon and Breach, Montreux, pp. 23–95.

Cai, Tao, 2016. A semi-implicit spectral method for compressible convection of rotating and density-stratified flows in cartesian geometry. J. Comput. Phys. 310, 342–360.

Das, Shyam S., et al., 2012. CFD analysis of thermal stratification and sensitivity study of model parameters for k–ϵ model in a cylindrical hot plenum. Nucl. Eng. Des. 250, 417–435.

Gershuni, G.Z., Zhukhovitskii, E.M., 1969. Stability of plane-parallel convective motion with respect to spatial perturbations: PMM vol. 33, n5, 1969, pp. 855–860. J. Appl. Math. Mech. 33 (5), 830–835.

Hesthaven, J.S., Rozza, G., Stamm, B., et al., 2016. Certifiedreduced Basis Methods for Parametrized Partial Differ-ential Equations. Springer.

Hu, Rui, 2017. Development of a reduced-order three-dimensional flow model for thermal mixing and stratification simulation during reactor transients.

Ieda, Y., Maekawa, I., Muramatsu, T., et al., 1990. Experimental and analytical studies of the thermal stratification phenomenon in the outlet plenum of fast breeder reactors. Nucl. Eng. Des. 120 (2–3), 403–414.

Ingersoll, Andrew P., 1966. Convective instabilities in plane Couette flow. Phys. Fluids 9 (4), 682–689.

Langhans, Robert, 2017. Liquid Sodium Stratification Prediction and Simulation in a Two-Dimensional Slice (MS thesis). Technische Universität.

Lee, I.S., Suh, K.Y., 2006. HELIOS for thermal-hydraulic behavior of Pb-Bi cooled fast reactor PEACER. No. IAEA-TECDOC–1520.

Merzari, Elia, Obabko, Aleks, Fischer, Paul, Halford, Noah, Walker, Justin, Siegel, Andrew, Yu, Yiqi, 2017. Large-scale simulation of nuclear reactors: issues and perspectives. 312, (FEB.), pp. 86–98.

Moriya, Shoichi, et al., 1987. Effects of Reynolds number and Richardson number on thermal stratification in hot plenum. Nucl. Eng. Des. 99, 441–451.

Ohira, H., et al., 2013a. Benchmark analyses of sodium natural convection in the upper plenum of the MONJU reactor vessel. In: International Conference on Fast Reactors and Related Fuel Cycles: Safe Technologies and Sustainable Scenarios (FR13). IAEA-CN-199/142.

Ohira, H., et al., 2013b. Benchmark analyses of sodium natural convection in the upper plenum of the MONJU reactor vessel. In: Int. Conf. Fast Reactors and Related Fuel Cycles: Safe Technologies and Sustainable Scenarios–FR, Vol. 13.

Ohno, S., Ohki, H., Sugahara, A., et al., 2011. Validation of a computational simulation method for evaluating thermal stratification in the reactor vessel upper plenum of fast reactors. J. Nucl. Sci. Technol. 48 (2), 205–214.

Opanasenko, A.N., 1988. Coolant stratification in nuclear power plant pipes. 65 (1). pp. 623–625.

Opanasenko, A.N., et al., 2012. Coolant stratification in nuclear power facilities. At. Energy 111 (3), 172–178.

Peng, T.J., Gu, Long, DWe, W., 2017. Conceptual design of subcritical reactor for China initiative accelerator driven system. At. Energy Sci. Technol. 51 (12), 2235–2241.

Roelofs, F., Gopala, V.R., Tichelen, K.V., et al., 2013. Status and future challenges of CFD for liquid metal cooled reactors. Iaea Fr.

Sakamoto, T., Shibahara, M., Takata, T., Yamaguchi, A., 2010. Numerical study of three dimensional thermal hydraulics effect on thermal stratification phenomena in upper plenum of MONJU. In: Proc. Korea-Japan Symposium on Nuclear Thermal Hydraulics and Safety. NTHAS7.

Sehgal, B.R., Ma, W.M., 2006. Thermal-hydraulic ADS lead bismuth loop (TALL) and experiments on a heat exchanger BR Sehgal, WM MA, A. Karbojian. In: Theoretical and Experimental Studies of Heavy Liquid Metal Thermal Hydraulics. p. 259.

Tenchine, D., 2010. Some thermal hydraulic challenges in sodium cooled fast reactors. Nucl. Eng. Des. 240 (5), 1195–1217.

Tenchine, D., et al., 2013. Experimental and numerical studies on mixing jets for sodium cooled fast reactors. Nucl. Eng. Des. 263, 263–272.

Visser, D.C., Keijers, S., Lopes, S., et al., 2020. CFD analyses of the European scaled pool experiment E-SCAPE. Nucl. Eng. Des. 358, 110436.

Wu, Ke, Welfert, Bruno D., Lopez, Juan M., 2018. Complex dynamics in a stratified lid-driven square cavity flow. J. Fluid Mech. 855, 43–66.

Yanez, J., Class, A.G., 2019. POD-ROM verification of the accuracy of the simulation of a heated pool. In: The Proceedings of the International Conference on Nuclear Engineering, Vol. 2019, No. 27. ICONE, p. 2390.